ARCHIVES OF ELECTRICAL ENGINEERING VOL. 74(1), pp. 291 –309 (2025)

DOI 10.24425/aee.2025.153025

Analytical model of a cylindrical linear module with permanent magnet based on approximation functions

SEBASTIAN JAN BARTEL ✉, KRZYSZTOF KLUSZCZYŃSKI

Cracow University of Technology
Warszawska 24, 31-155 Kraków, Poland
e-mail: {✉ sebastian.bartel/krzysztof.kluszczynski}@pk.edu.pl

(Received: 11.09.2024, revised: 10.02.2025)

Abstract: The authors of the paper analyse and carry out simulation studies on a cylindrical linear "excitation coil – permanent magnet" module, which is an elementary component of many electromagnetic devices and linear permanent magnet (PM) electric motors. The geometric dimensions of the module and the winding data of the excitation coil correspond to the constructed prototype. The most important result of the work is demonstrating that it is possible to approximate the discrete function of the electromagnetic force acting on the runner, the flux linked with the excitation coil and the electromotive force of motion induced in the excitation coil using a modified Kloss function. The consequence of these approximations is conversion of the classical field-circuit model with Lookup Tables into a purely analytical model. Using this model, simulation studies of the oscillatory motion of the runner were carried out in the MATLAB Simulink environment, confirming the usefulness of the developed analytical model in the numerical analysis of dynamic states.

The next part is dedicated to the experimental verification of the proposed analytical mathematical model. A laboratory setup with a high-speed camera was designed and built.

A comparative analysis of the time curves obtained from measurement studies and simulation studies was conducted using the example of the damped oscillatory motion of the runner. The root mean square errors (RMSEs) were determined for various time intervals, relevant from the perspective of implementing the developed analytical mathematical model in control systems of different linear electromagnetic devices with permanent magnets.

Key words: analytical form of field-circuit model, approximation of various electromagnetic quantities, "excitation coil – PM runner" module, linear PM electromagnetic devices, modified Kloss function

1. Introduction

The dynamic development of neodymium permanent magnet manufacturing technology and the constant improvement of magnet performance parameters have led to the increasingly widespread use of permanent magnets in electric motors and actuators. This applies to both rotary and linear electromechanical converters [3,8–10,13,15,16,19–21]. The development of technology for drives with permanent magnets is accompanied by the remarkable advancement in design methods of such converters which base usually on circuit-field and field calculations [1,5,6,11,12,17,18,22–24]. This article concerns a cylindrical linear "single excitation coil – permanent magnet" module, which is an elementary component of many electromagnetic devices, particularly those in which the magnetic field generated in the air around the considered modules does not interfere with the operation of other devices. The main aim is to indicate the possibility of a new approach to formulating mathematical models of the electromagnetic devices containing the above-mentioned module or consisting of such modules based on the use of analytical approximation functions.

A modified Kloss function was chosen as the approximation function, which has not previously appeared in this form in the known technical literature and has not been used for such purposes. The first indication that it can be used to describe the electromagnetic force is contained in the [2].

2. Description of the constructed cylindrical linear "single excitation coil – permanent magnet" module

The analysed cylindrical linear "single excitation coil – permanent magnet" module is schematically presented in Fig. 1. As mentioned, such a module (or a set of such modules) is part of various electromagnetic devices or linear electric motors.

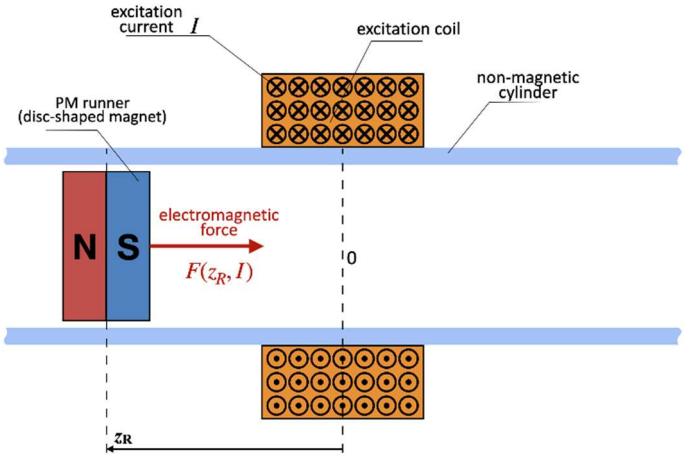

Fig. 1. Schematic diagram of a cylindrical linear "single excitation coil – permanent magnet" module (with disc-shaped PM)

The permanent magnet (disc-shaped or ring-shaped) serves as the runner which moves within the cylinder under the influence of the magnetic field generated by the energised excitation coil wound around the cylinder. The cylinder is made of a non-magnetic material (e.g. Teflon, a synthetic polymer material or filament used in 3D printing technology).

The position of the runner relative to the excitation coil is determined by the coordinate z_R (Fig. 1).

The following terminology and designations of the geometric dimensions of the individual elements of the considered module are adopted: outer radius of the permanent magnet R_R, length of the permanent magnet L_R, inner radius of the permanent magnet r_R (if the permanent magnet is ring-shaped), length of the excitation coil L_C, inner radius of the excitation coil r_C, outer radius of the excitation coil R_C, length of the cylinder C_l and wall thickness of the cylinder C_d.

This occurs:

$$H_C - R_C - r_C, \tag{1}$$

where H_C is the cross-sectional height of the excitation coil.

The authors designed a prototype in which they assumed a ratio of the excitation coil height H_C to its length L_C equal to 1:1 ($H_C/L_C = 1$) based on the conclusions drawn from a comparative analysis of coils with different proportions conducted in [3, 5, 6]. Taking into account these conclusions, the geometric dimensions of the permanent magnet and the excitation coil of the designed and constructed module have proportions and dimensions, as shown in Fig. 2. Regarding the cylinder, its length and its wall thickness are, respectively: $C_l = 120$ mm and $C_d = 1.6$ mm. The inner radius of the cylinder is matched to the outer radius of the permanent magnet R_R to ensure a sliding fit.

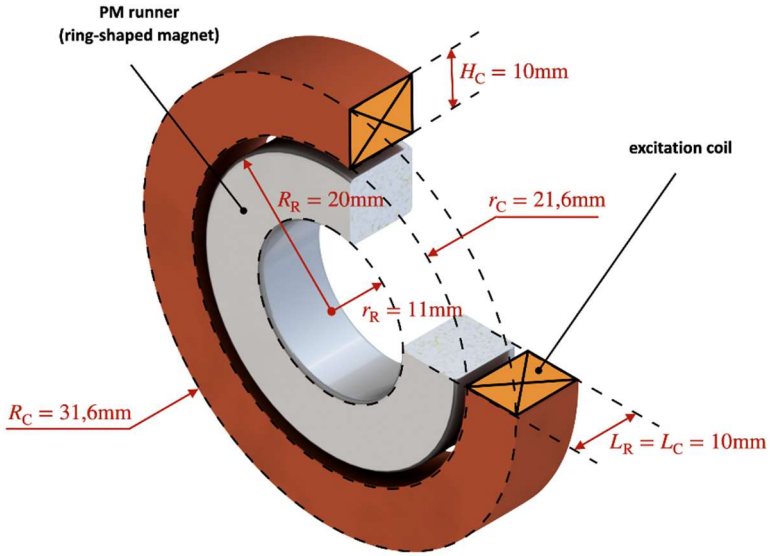

Fig. 2. Visualisation of the "single excitation coil – permanent magnet" module having a ratio of $H_C/L_C = 1$ (with ring-shaped PM)

The number of turns of the excitation coil is $n = 576$. The excitation coil is made of insulated AWG 26 winding wires (American Wire Gauge) with a diameter of 0.4 mm and its filling factor is 74%. The cylinder is made of Teflon and the permanent magnet is made of N38 neodymium. Based on the insulation class, wire diameter and cooling conditions, the maximum (allowable) excitation current density is set at 4 A/mm^2, corresponding to a maximum excitation current of 0.7 A ($I_{\max} = 0.7$ A).

3. Mechanical and electrical equilibrium equations of the cylindrical "single excitation coil – permanent magnet" module

The mathematical model of the cylindrical "single excitation coil – permanent magnet" module includes:

– mechanical equilibrium equations (for the runner)

$$m\frac{\mathrm{d}^2 z_R}{\mathrm{d}t^2} - F - F_m - F_t,$$
$$F_t - k_t \cdot \operatorname{sgn}\left(\frac{\mathrm{d}z_R}{\mathrm{d}t}\right), \tag{2}$$

where: m is the mass of the runner, F is the electromagnetic force acting on the runner dependent on the current value and the runner's position, F_m is the load force, F_t is the friction force between the runner and the inner surface of the cylinder, k_t is the friction coefficient (it was assumed that the aerodynamic drag force can be neglected),

– electrical equilibrium equations (for the excitation coil)

$$u_z - R \cdot i + L\frac{\mathrm{d}i}{\mathrm{d}t} - e_{\mathrm{mov}}, \tag{3}$$

where: u_z is the voltage waveform of the excitation coil power supply, R is the resistance of the excitation coil, i is the instantaneous current value in the excitation coil, L is the self-inductance of the excitation coil, e_{mov} is the electromotive force of motion induced in the excitation coil (regarded as a source) dependent on the position and speed of the runner,

– and initial conditions that are:

$$z_R\,(t = 0) = z_{R0}, \tag{4}$$
$$\frac{\mathrm{d}z_R}{\mathrm{d}t} = v\,(t = 0) = v_0. \tag{5}$$

The above system of differential equations composed of Eqs. (4) and (5) after transforming to canonical form can be rewritten in the following way:

$$\frac{\mathrm{d}^2 z_R}{\mathrm{d}t^2} - \frac{1}{m} \cdot (F - F_t - F_m), \tag{6}$$
$$\frac{\mathrm{d}i}{\mathrm{d}t} = \frac{1}{L} \cdot (u_z - R \cdot i - e_{\mathrm{mov}}). \tag{7}$$

4. Approximation of the discrete function of the electromagnetic force and the electromotive force of motion

The classical method for solving the above system of differential equations (Eqs. (6) and (7)) involves turning the mathematical model into a field-circuit model, where the relationship between the electromagnetic force F and two variables: the position z_R and excitation current I, as well as the relationship between the electromotive force of motion induced in the excitation coil $e_{\mathrm{mov}}(t)$ and two variables: the position z_R and the runner speed v are discrete functions determined on the basis of field calculations. The results of these field calculations for appropriately selected points of the runner position, instantaneous excitation current values and runner speeds are compiled into the so-called Lookup Tables, which form an essential part of the model [1, 7, 12, 14].

The new method of solving the mathematical model involves transforming it into a purely analytical model by replacing the discrete functions of electromagnetic force and electromotive force of motion with their approximations.

The method of approximating the electromagnetic force using a modified Kloss function is presented in [2–4]. For the constructed prototype (Figs. 1 and 2), the discrete function of the electromagnetic force determined by the field method (using the FEMM 4.2 software) for 320 points, under the assumption that the excitation coil current i is constant: $i = I$ and equal to maximum allowable value $I = I_{\max} = 0.7$ A, is shown in Fig. 3.

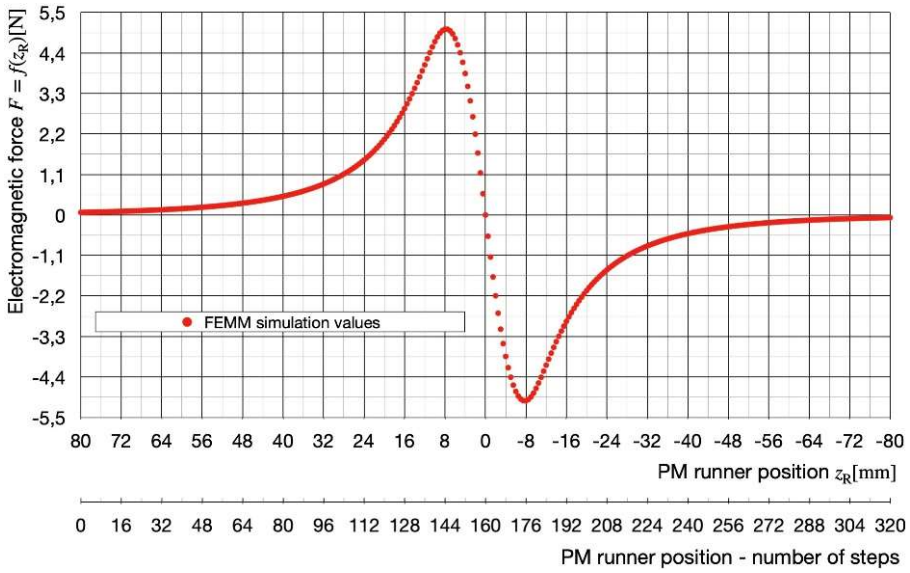

Fig. 3. The discrete function of the electromagnetic force determined by the field method (using the FEMM 4.2 software) for 320 points assuming that the constant excitation coil current value is at its maximum: $I_{\max} = 0.7$ A

Due to the linearity of the magnetic circuit, the relationship between the electromagnetic force, the spatial coordinate z_R and the excitation current i can be reduced to the product of the linear function $\frac{i}{I_{\max}}$ and the discrete function $f(z_R, I = I_{\max})$ shown in Fig. 3:

$$F(z_R, i) - \frac{i}{I_{\max}} f(z_R, I - I_{\max}). \tag{8}$$

The function approximating the discrete function $f(z_R, I = I_{\max})$, which is described in detail in [2–4] is a modified Kloss function having the following form:

$$f(z_R, I = I_{\max}) = \frac{M' z_R}{\left(S' + z_R^2\right)^2}. \tag{9}$$

The coefficients of the above analytical function for the discrete function shown in Fig. 3, determined using the Hooke-Jeeves optimisation algorithm, are: $M' = -34387$ and $S' = 172$.

Therefore, the electromagnetic force acting on the runner in the constructed prototype can be described (based on relations (8) and (9)), as follows:

$$F(z_R, i) - \frac{i}{I_{\max}} \cdot \frac{M' z_R}{\left(S' + z_R^2\right)^2} - \frac{i}{0.7} \cdot \frac{(-34387) \cdot z_R}{\left(172 + z_R^2\right)^2}. \tag{10}$$

In order to determine analytically the electromotive force of motion induced in the excitation coil by the permanent magnet, it is necessary to approximate the distribution of the flux linked with the excitation coil as a function of the runner position $\Psi(z_R)$. The discrete distribution of the flux linked with the excitation coil $\Psi(z_R)$ determined using the field method (in the FEMM 4.2 program), in a manner analogous to that used to determine the distribution of the electromagnetic force (Fig. 3), is shown in Fig. 4.

To achieve consistency between the analytical description of the flux distribution linked with the excitation coil (Fig. 5) and the analytical description of the electromagnetic force (Eq. (10)), it was decided to consider the function $g(z_R)$ as the approximation function, which is the indefinite integral of the modified Kloss function described by the formula:

$$g(z_R) = \int f(z_R)\, \mathrm{d}z_R = \frac{M''}{2\left(S'' + z_R^2\right)} \tag{11}$$

The impact of the coefficients M" and S'' on the shape of the function $g(z_R)$ is illustrated in Fig. 5.

Comparing the analytical functions presented in Fig. 5 with the discrete function shown in Fig. 4, it can be noticed that the analytical function $g(z_R)$ (Eq. (11)) correlates very well with the waveform of the discrete flux function.

The coefficients M'' and S'' of the analytical function $g(z_R)$ (Eq. (11)), approximating the discrete flux function as depicted in Fig. 4, were determined (similarly to the electromagnetic force) using the Hooke-Jeeves optimisation algorithm. They are: $M'' = 52.2$ and $S'' = 181.6$.

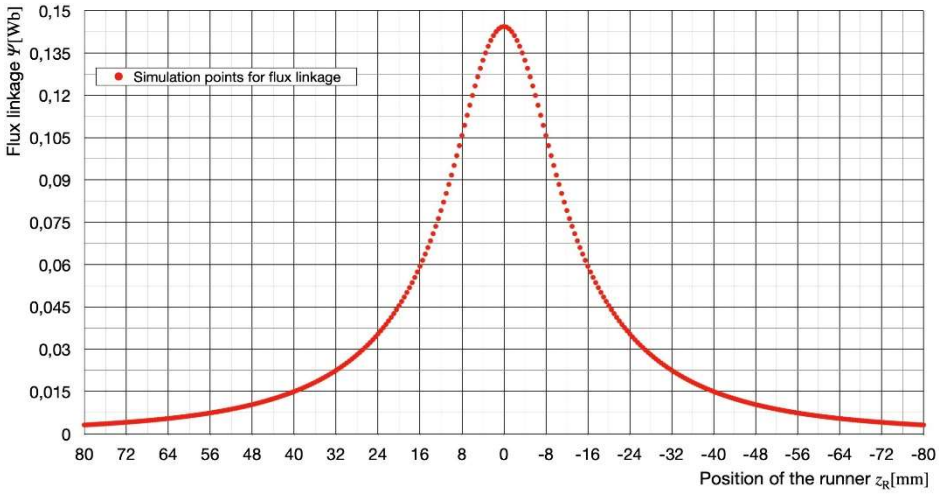

Fig. 4. The discrete function of the electromotive force of motion induced in the excitation coil by the permanent magnet was determined by the field method (using the FEMM 4.2 software) for 320 points of the runner position

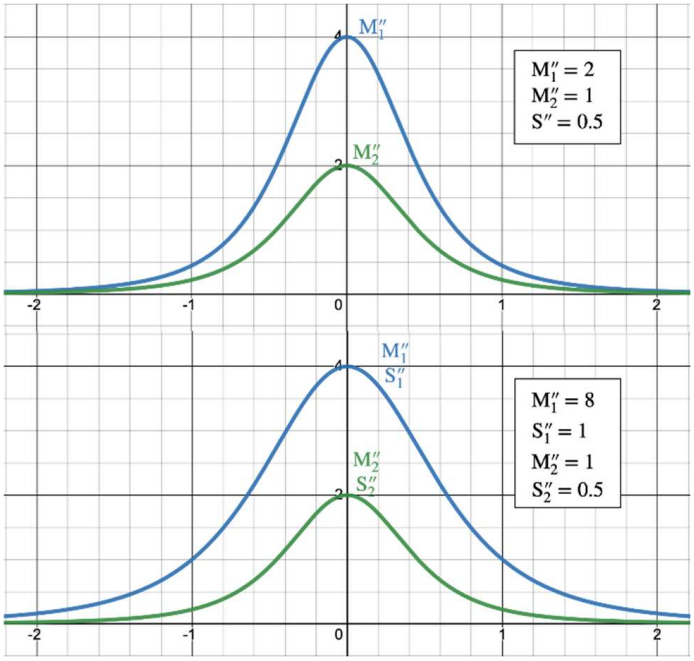

Fig. 5. The influence of coefficients M'' and S'' on the shape of the function $g(z_R)$, approximating the discrete function of the flux linked with the excitation coil

With these values of both coefficients, the function approximating the discrete flux function linked with the excitation coil (Fig. 4) of the form:

$$\Psi(z_R) = \frac{M''}{2\left(S'' + z_R^2\right)} = \frac{52.2}{2\left(181.6 + z_R^2\right)}. \tag{12}$$

has a root mean square error RMSE of 0.001 and a percentage error $\varepsilon = 1.5\%$, which means that the function being an integral of the modified Kloss function was very well chosen for approximating the flux linked with the excitation coil. This is confirmed by Fig. 6.

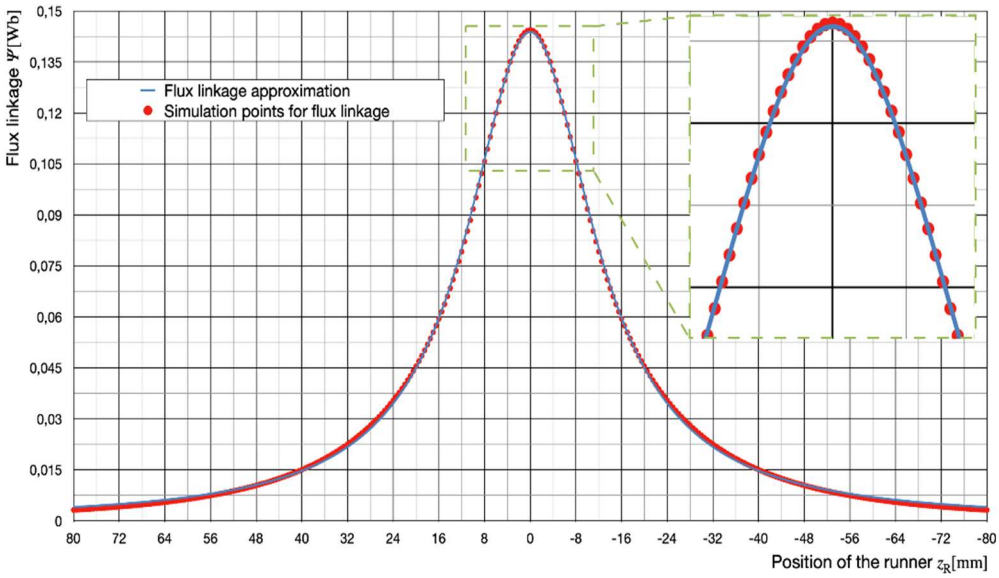

Fig. 6. Comparison of the discrete function of the flux linked with the excitation coil with the approximation function based on the indefinite integral of the modified Kloss function (Eq. (11))

With the above analytical description of the flux linked with the excitation coil, we can analytically determine the electromotive force of motion induced in the excitation coil by the permanent magnet:

$$e_{\text{mov}}(t) = -\frac{\mathrm{d}\Psi(z_R)}{\mathrm{d}t} = -\frac{\mathrm{d}z_R}{\mathrm{d}t}\frac{\mathrm{d}\Psi(z_R)}{\mathrm{d}z_R} = -\frac{\mathrm{d}z_R}{\mathrm{d}t}\frac{M''z_R}{\left(S'' + z_R^2\right)^2},$$
$$e_{\text{mov}}(t) = -v(t)\frac{M''z_R}{\left(S'' + z_R^2\right)^2}, \tag{13}$$

where $\Psi(Z_R)$ is the flux linked with the excitation coil generated by the permanent magnet and v is the linear velocity of the runner.

Substituting the previously determined values of the coefficients M'' and S'', we obtain the final expression for the electromotive force, as follows:

$$e_{\text{mov}}(t) = -\nu \frac{52.3 \cdot z_R}{\left(181.6 + z_R^2\right)^2}. \tag{14}$$

5. The analytical mathematical model of a cylindrical "single excitation coil – permanent magnet" module

Introducing the electromagnetic force described by Eq. (10) and the electromotive force of motion described in Eq. (14) into the system of differential equations: Eqs. (2) and (3) we obtain the mathematical model of the considered cylindrical "single excitation coil – permanent magnet" module (presented in Figs. 1 and 2) in the following purely analytical form:

$$\frac{\mathrm{d}^2 z_R}{\mathrm{d}t^2} = \frac{1}{m} \cdot \left(\frac{i}{0.7} \cdot \frac{(-34387) \cdot z_R}{(172 + z_{R^2})^2} - F_t - F_m \right), \tag{15}$$

$$\frac{\mathrm{d}i}{\mathrm{d}t} = \frac{1}{L} \cdot \left(u_z - R \cdot i + \nu \frac{52.2 \cdot z_R}{(181.6 + z_{R^2})^2} \right). \tag{16}$$

The block diagram of the analytical mathematical model of the "single excitation coil – permanent magnet" module is presented graphically in Fig. 7.

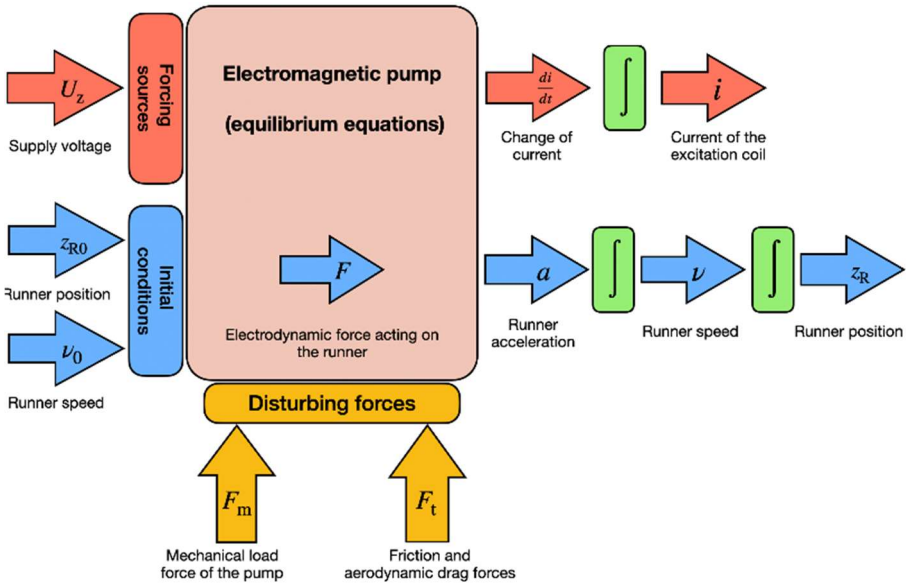

Fig. 7. The graphical structure of the mathematical model of the "single excitation coil – permanent magnet" module describing input variables, output variables and disturbance variables

The simulation model was elaborated in the MATLAB Simulink environment. The graphical structures of the differential equations: mechanical equilibrium equation (Eq. (6)) and electrical equilibrium equation (Eq. (7)) with initial conditions given by Eqs. (4) and (5), are presented in Figs. 8 and 9, respectively.

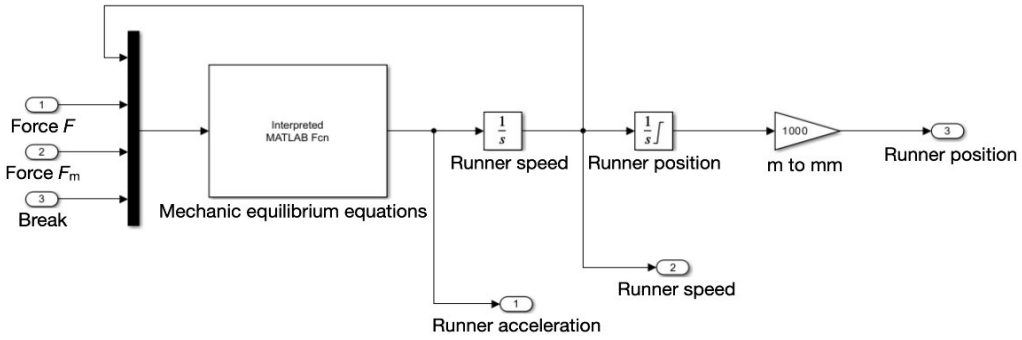

Fig. 8. The structure of the mechanical equilibrium equation after implementation in the MATLAB Simulink environment

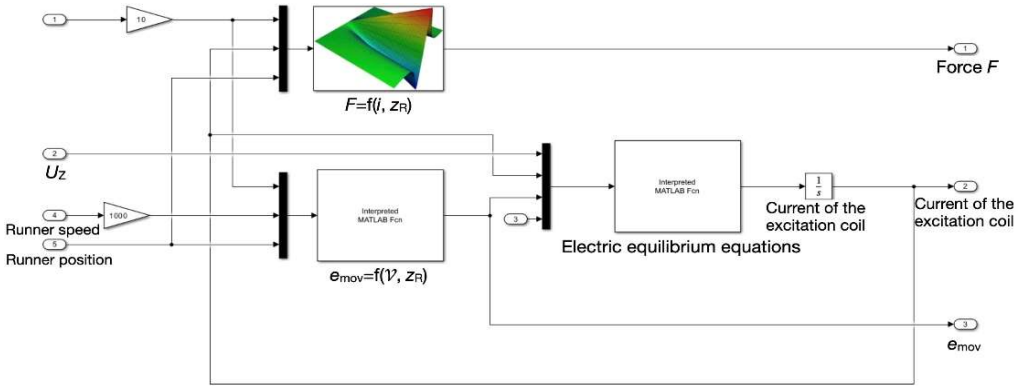

Fig. 9. The structure of the electrical equilibrium equation after implementation in the MATLAB Simulink environment

The excitation coil resistance is $R = 13.8\ \Omega$ and the mass of the runner (the mass of the ring-shaped permanent magnet) is $m = 65.71$ g. The self-inductance of the excitation coil determined by the field method is $L = 20.9$ mH.

6. Simulation studies of the oscillatory motion of the runner based on the analytical mathematical model of the "single excitation coil – permanent magnet" module

The simulation studies were conducted under the assumption that the excitation coil is powered by a step voltage $u_z(t) = U_z \cdot 1(t)$, and the initial condition for the runner position is $z_{R0} = 10$ mm. It is evident that in this scenario, the motion of the runner released at the moment $t = 0$ will be damped oscillatory motion.

For all the analysed cases a constant friction force was assumed to be $F_t = 0.137$ N (estimated on the basis of laboratory experiments). The simulation model of the cylindrical module was solved for 4 different cases differing in the excitation coil voltage: $U_z = 8$ V and $U_z = 16$ V at the no-load state $F_m = 0$ N and the full load $F_m = 2$ N. For each case the following time curves were determined: runner acceleration $a(t)$, runner velocity $v(t)$, runner position $z_R(t)$ and excitation coil current $i(t)$.

The considered 4 cases are as follows:

case 1: $U_z = 8$ V, $z_{R0} = 10$ mm, no-load state $F_m = 0$ N;

case 2: $U_z = 6$ V, $z_{R0} = 10$ mm, no-load state $F_m = 0$ N;

case 3: $U_z = 8$ V, $z_{R0} = 10$ mm, full load $F_m = 2$ N;

case 4: $U_z = 16$ V, $z_{R0} = 10$ mm, full load $F_m = 2$ N.

Simulation results in the form of time curves for the acceleration a(t), velocity $v(t)$ and position $z_R(t)$ of the runner, along with the excitation coil current $i(t)$ for the last case 4, chosen as the example, are presented in Fig. 10.

For all the simulated cases 1, 2, 3 and 4 the time required for the runner to move from its initial position to the centre of the excitation coil ΔT (half of the first oscillation) and the oscillation decay time of the runner ΔT_{mech} have been determined. How to determine these characteristic times ΔT and ΔT_{mech} was shown on the example of two representative cases in Fig. 11 (the case in Fig. 11(a): $U_z = 16$ V, $z_{R0} = 40$ mm and $F_m = 0$ N; the case in Fig. 11(b): $U_z = 10$ V, $z_{R0} = 10$ mm and $F_m = 0.2$ N).

The characteristic times ΔT and ΔT_{mech} read in this manner for all the considered cases 1, 2, 3 and 4 (solved with use of Kloss function approximation) are put together in Table 1.

Table 1. Characteristic times ΔT and ΔT_{mech} for the 4 considered cases

F_m [N]	U_Z [V]	ΔT [ms]	ΔT_{mech} [ms]
0	8	23	360
	16	16	455
2	8	39	185
	16	19	365

The analysis of the results presented in Table 1 confirms that for the same load F_m, increasing the voltage U_z results in a shorter characteristic time ΔT, whereas increasing the load F_m at the same voltage U_z leads to a longer characteristic time ΔT. Similarly, increasing the voltage U_z for the same load F_m results in a longer oscillation decay time ΔT_{mech}, while increasing the load

F_m for the same voltage U_z results in a shorter oscillation decay time ΔT_{mech}. This allows us to conclude that the new model based on the modified Kloss function as the approximation function is qualitatively accurate. The quantitative assessment of this model is presented in the next chapter.

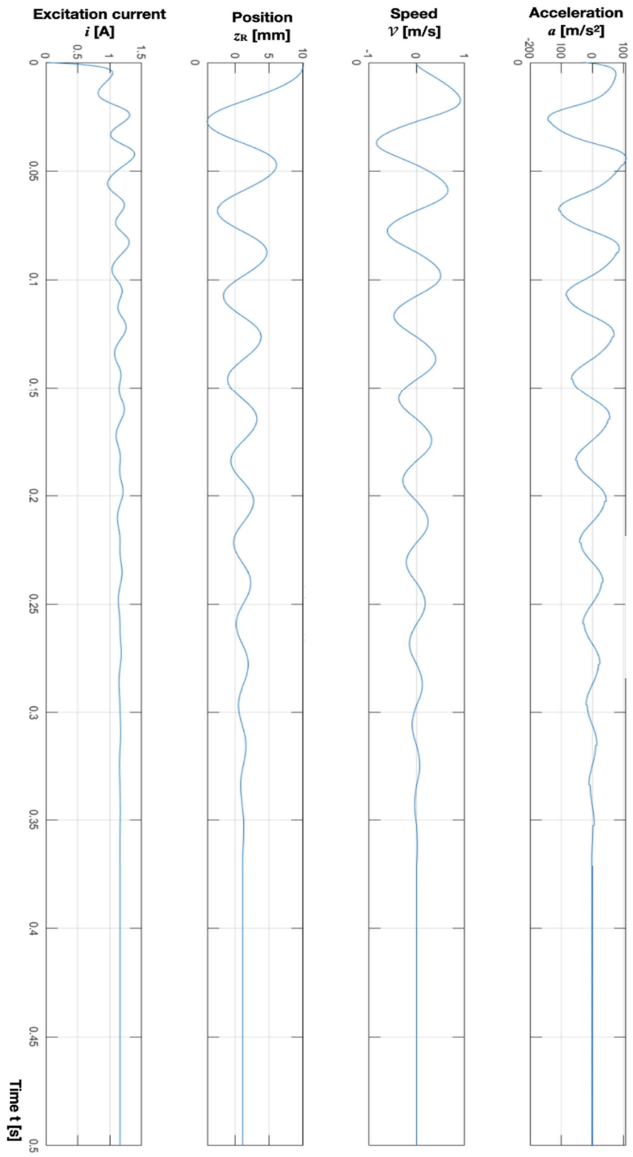

Fig. 10. Time curves for runner acceleration, runner velocity, runner position and excitation coil current for the chosen case 4: $U_z = 16$ V, $z_{R0} = 10$ mm and full load $F_m = 2$ N determined on the basis of analytical mathematical model

Fig. 11. Method of determining the characteristic times ΔT and ΔT_{mech} for 2 exemplary cases: (a) $U_z = 16$ V, $z_{R0} = 40$ mm and $F_m = 0$ N; (b) $U_z = 10$ V, $z_{R0} = 10$ mm and $F_m = 0.2$ N

7. Description of the laboratory stand for measuring instantaneous position of the runner

The schematic diagram of the laboratory stand for measuring the instantaneous position of the runner in the "single excitation coil – permanent magnet" module using a high-speed camera is shown in Fig. 12.

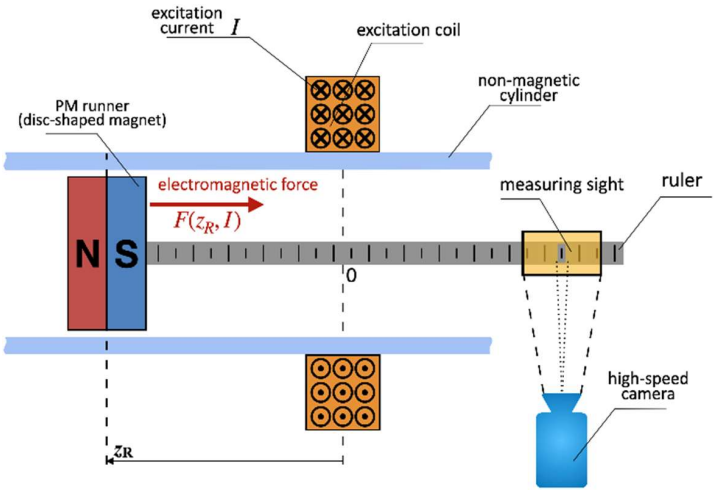

Fig. 12. The schematic diagram of the laboratory stand for measuring instantaneous position of the runner with use of a high-speed camera

The laboratory stand consists of a measurement ruler rigidly connected to the runner, a viewer for optically reading the instantaneous position of the runner z_R and a high-speed camera embedded in a mobile device from Apple Inc., mounted on a suitably chosen rigid metal tripod. A photo of the laboratory stand elaborated according to this concept is shown in Fig. 13.

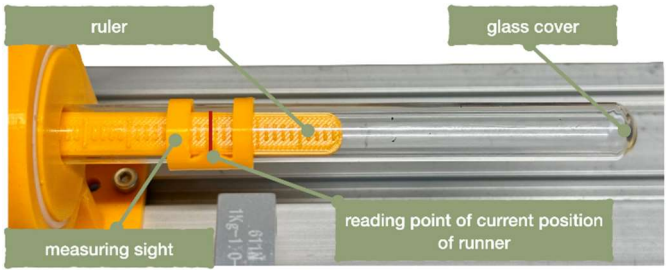

Fig. 13. Laboratory stand for measuring the instantaneous position of the runner in the cylindrical linear module (photo)

The camera used to record the runner motion was equipped with a 48 MP Sony sensor, a 7-element lens with a 24 mm focal length, an aperture of $f/1.78$ and automatic four-axis Optical Image Stabilisation (OIS). The recorded image with a resolution of Full HD (1920 × 1080 px), was saved in RAW format at a speed of 240 frames per second.

The measurement verification was conducted using the example of the runner oscillatory motion. The runner was placed in the initial position $z_{R0} = 40$ mm. The excitation coil was powered by a step voltage $u_z(t) = U_z \cdot 1(t)$, where $U_z = 9.7$ V. The shape of the required step voltage was checked experimentally. Under the influence of the magnetic field generated by the energised excitation coil, the runner, released at the moment $t = 0$ from the initial position $z_{R0} = 40$ mm, performed damped oscillatory motion. This motion was recorded by the camera until the runner came to a stop. In the experiment, the transient state lasted approximately 0.45 seconds, and the number of frames recorded at a speed of 240 frames per second was about 110 frames. To obtain the instantaneous position of the runner, the recorded frames were analysed frame by frame. The results of the measurements supplemented by simulation results obtained on the basis of the developed analytical mathematical model are presented in the same Fig. 14.

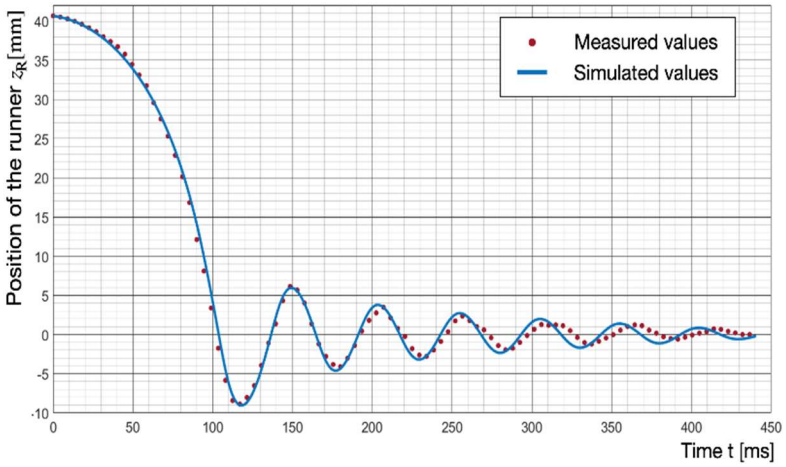

Fig. 14. Comparison of the time curve for runner position determined experimentally with the curve obtained through simulation based on the proposed analytical mathematical model ($U_Z = 10$ V and $z_{R0} = 40$ mm)

The percentage error ε for the entire duration of the transient state $t \in (0 \div 450)$ ms is $\varepsilon = 11.9\%$ (with the simulation as a reference). The difference between the simulated and measured runner positions increases with time, and the reason for this is that the aerodynamic drag force whose value decreases as the speed of the runner decreases, was neglected in the simulation studies. It is necessary to underline that in the control systems of various linear electromagnetic devices with permanent magnets, the re-switching of the excitation coils takes place in much shorter time intervals. Considering the potential implementation of the proposed analytical mathematical model in such control systems, the error ε was determined for two shorter time intervals: $t \in (0 \div 104)$ ms and $t \in (0 \div 217)$ ms, as depicted in Fig. 15.

For the time interval $t = 0 \div 217$ ms, the error ε is 5.6% while for the interval $t = 0 \div 104$ ms, the error ε is even less – $\varepsilon = 3.0\%$, (latter time intervals correspond to the re-switching times of excitation coils in electromagnetic devices with several excitation coils [8, 9, 19]).

The above percentage errors (in the range of only a few percent) indicate that the proposed analytical model can be successfully implemented in different control systems.

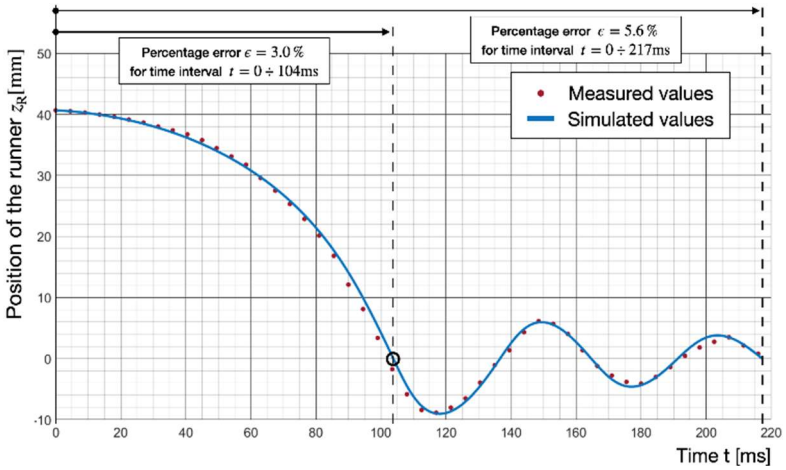

Fig. 15. Determination of the percentage errors ε for shorter time intervals: $t \in (0 \div 104)$ ms and $t \in (0 \div 217)$ ms

In the next step, it was decided to verify the correctness of the developed analytical model in yet another way. For the measured time curve from Fig. 4, a time plot of the absolute value positions of the runner $|z_R|$ was drafted (red dashed line) and then all consecutive maximum points (marked with yellow symbols "?" in Fig. 16) were connected together by an exponential curve. The final result of this graphical procedure, illustrating the so-called trend line of the damping oscillatory motion of the runner is presented in Fig. 16.

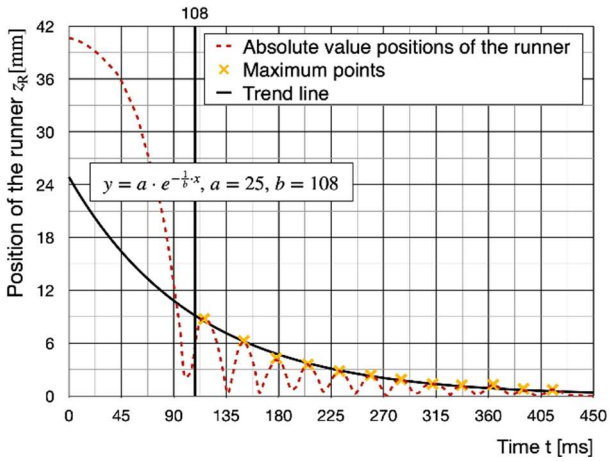

Fig. 16. Graphical procedure for determining trend line of the damping oscillatory motion of runner

The trend line shown in Fig. 16 can be described by the following equation:

$$y - a \cdot e^{-\frac{1}{b} \cdot x}, \quad a = 25, \quad b = 108. \tag{17}$$

The coefficient b is equal to the time constant which in the considered case takes the value $\tau_R = 108$ ms. Also, from such a point of view, taking into account the trend line of the damping oscillatory motion of the runner and the associated with this line time constant τ_R, the measurement experiments align well with the results of the simulation studies, as shown in Fig. 17.

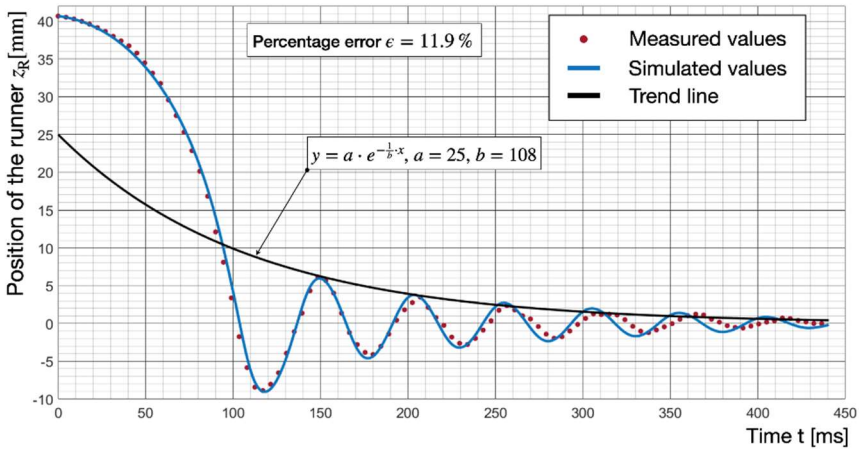

Fig. 17. Comparison of the trend lines of the damping oscillatory motion of runner obtained on the basis of experiment simulation

8. Conclusions

The subject of theoretical analysis, simulation studies and laboratory experiments was the cylindrical linear "single excitation coil – permanent magnet" module which is an elementary component of many electromagnetic devices and linear PM electric motors. By approximating the discrete function of the electromagnetic force acting on the runner using an analytical function based on the modified Kloss function and subsequently approximating the discrete function of the flux linked with the excitation coil using an analytical function based on the indefinite integral of the modified Kloss function, it was demonstrated that the classical mathematical model of the analysed module, in the form of a field-circuit model with Lookup Tables, can be replaced by a purely analytical model. The method of solving such an analytical model in the MATLAB Simulink environment was illustrated using the example of the oscillatory motion of the runner under different conditions of excitation coil supply, both in a no-load state and at full load.

The presented comparison of the experimental results obtained when using a high-speed camera on the laboratory stand with the results of simulations based on the elaborated analytical mathematical model of the "single excitation coil – permanent magnet" module indicates fully satisfactory agreement. This agreement has been confirmed through comparative analysis from various perspectives: direct comparison of time curves by calculating percentage errors ε over different time intervals, comparison of the trend lines of the damping oscillatory motion of the runner and comparison of time constants of these lines. It shows that the analytical mathematical model is suitable for implementation in control systems of electromagnetic devices with permanent magnets [10, 16, 17].

"Single excitation coil – permanent magnet" module is a component of a wide variety of electromagnetic devices and electromechanical converters, so it will be useful to consider in future the problems associated with the efficiency of such a module and the density of the generated force (described by the force-per-mass ratio and force-per-volume ratio), as well as minimisation of the module mass and volume following, for example, the detailed analysis made in [14] in relation to magnetorheological disc brakes.

It is also worth mentioning that the proposed measurement method using a high-speed camera has proven to be effective. Its advantages include the low cost of the laboratory stand, easy operation and the ability to perform multiple measurements quickly and easily within a short time interval.

The authors envisage the application of the presented "single excitation coil – permanent magnet" module in the development of the model of a linear cylindrical electromagnetic pump, whose permanent magnet (runner) simultaneously performs the function of the piston and in the model of an electromagnetic launcher with missiles made of permanent magnets.

In order to facilitate the use of the new model by designers of such electromagnetic devices, they plan at a later stage to determine the relationships between the M'' and S'' coefficients of the approximating function used and the constructional data of the module (geometrical dimensions, number of turns of the excitation coil, specification of the permanent magnet).

References

[1] Barba P.D., Savini A., Wiak S., *Field models in electricity and magnetism*, Springer (2008), DOI: 10.1007/978-1-4020-6843-0.

[2] Bartel S., Kluszczyński K., *Approximation of electromagnetic force axial distribution in "single excitation coil – PM runner" module based on modified Kloss function*, Archives of Electrical Engineering (in print), no. 4 (2024).

[3] Bartel S., *Electromagnetic pump with programmable performance characteristics with a permanent magnet synchronous linear motor*, PhD thesis, Cracow University of Technology (in Polish, supervisor: professor Krzysztof Kluszczyński, PhD, DSc) (2024).

[4] Bartel S., Kluszczyński K., *Approximation of the function of electrodynamic force acting in a piston electromagnetic pump*, Przegląd Elektrotechniczny (in Polish), vol. 99, no. 1, pp. 179–184 (2023), DOI: 10.15199/48.2023.01.35.

[5] Bartel S., Kluszczyński K., *The Problem of Choosing the Optimal Ratio: Height to Length of Excitation Coil in Linear Cylindrical PM Synchronous Motors*, Progress in Applied Electrical Engineering (PAEE), Koscielisko, Poland, pp. 1–7 (2023), DOI: 10.1109/PAEE59932.2023.10244671.

[6] Bartel S., Kluszczyński K., *The issue of selecting the geometric proportions of excitation coils in a linear cylindrical synchronous motor with a permanent magnet as a running gear*, Przegląd Elektrotechniczny, vol. 100, no. 2, pp. 55–61 (2024), DOI: 10.15199/48.2024.02.10.

[7] Bernat J., Kołota J., Stępień G., Szymański G., *An inductance lookup table application for analysis of reluctance stepper motor model*, Archives of Electrical Engineering, vol. 60, no. 1, pp. 15–21 (2011), DOI: 10.2478/v10171-011-0002-y.

[8] Boldea I., *Linear Electric Machines, Drives, and MAGLEVs Handbook*, 2nd edition, CRC Press (2023), DOI: 10.1201/9781003227670.

[9] Cui F., Sun Z., Shen S., Xu W., Du G., *Design and Electromagnetic Characteristics Study of a High Speed and High Power Permanent Magnet Linear Synchronous Motor*, 2020 IEEE 9th International Power

Electronics and Motion Control Conference (IPEMC2020-ECCE Asia), Nanjing, China, pp. 1986–1991 2020, DOI: 10.1109/IPEMC-ECCEAsia48364.2020.9367781.

[10] Gieras A., Gieras J.F., *Recent Advancements in Permanent Magnet Motors Technology for Medical Applications*, Proceedings of Electrotechnical Institute, iss. 229 (2006).

[11] Gieras J.F., Shen J.X., *Modern permanent magnet electric machines: theory and control*, CRC Press – Taylor and Francis Group (2023), DOI: 10.1201/9781003103073.

[12] Glinka T., *Electric motors induced by permanent magnets*, Przegląd Elektrotechniczny (in Polish), ISSN: 2449-9544, 0033-2097, pp. 1–7 (2008).

[13] Guo K., Guo Y., *Optimization Design of Parallel Double Stator and Outer Mover Linear Rotary Permanent Magnet Machine Used for Drilling Robot*, 2020 IEEE International Conference on Applied Superconductivity and Electromagnetic Devices (ASEMD), Tianjin, China, pp. 1–2 (2020), DOI: 10.1109/ASEMD49065.2020.9276249.

[14] Kluszczyński K., Pilch Z., *The Choice of the Optimal Number of Discs in an MR Clutch from the Viewpoint of Different Criteria and Constraints*, Energies, vol. 14, iss. 21, 6888 (2021), DOI: 10.3390/en14216888.

[15] Komęza K., Pelikant A., Tegopoulos J., Wiak S., *Comparative computation of forces and torques of electromagnetic devices by means of different formulae*, IEEE Transactions on Magnetics, vol. 30, no. 5, pp. 3475–3478 (1994), DOI: 10.1109/20.312687.

[16] Kroczek R., *Design methodology, design issues, modeling and testing of hybrid electromagnetic launcher*, PhD thesis, Silesian University of Technology (in Polish, supervisor: professor Krzysztof Kluszczyński, PhD, DSc) (2009).

[17] Laithwaite E.R., *Linear electric motors*, Mills & Boon Limited (1971).

[18] Li P. *et al*., *The Research on Thrust Fluctuation Suppression Strategy of Electromagnetic Halbach Coreless Linear Motor*, 2023 IEEE International Conference on Applied Superconductivity and Electromagnetic Devices (ASEMD), Tianjin, China, pp. 1–2 (2023), DOI: 10.1109/ASEMD59061.2023.10369429.

[19] Loic Q., Ohsaki H., *Nonlinear abc-Model for Electrical Machines Using N-D Lookup tables*, IEEE Transactions on Energy Conversion, vol. 30, iss. 1 (2015), DOI: 10.1109/TEC.2014.2358854.

[20] Pawlak A.M. *Sensors and Actuators in Mechatronics: Design and Applications*, CRC Press (2007), DOI: 10.1201/9781315221632.

[21] Pawluk K., Szczepański W., *Electric linear motors*, Wydawnictwa Naukowo-Techniczne (in Polish) (1974).

[22] Prekaniak P., Pochanke A., Bodnicki M., *Computer simulation and experimental test of linear driver*, Machine Dynamics Research, no. 4, pp. 71–78, ISSN: 2080-9948 (2010).

[23] Wiak S., Napieralska-Juszczak E., *Computer field models of electromagnetic devices*, IOS Press BV (2010).

[24] Zawilak S., Zawilak T., *Medium power permanent magnet synchronous motors*, Zeszyty problemowe – Maszyny Elektryczne 1, Wrocław University of Science and Technology, no. 100, pp. 5–8 (2013).